Supporting Information

Deterministic Droplet-Based Co-Encapsulation of Single Cells through Inertial and Hydrodynamic Focusing

Byeong-Ui Moon[1], Lidija Malic[1*], Dillon Da Fonte[1], Liviu Clime[1], Félix Lussier[1,2], Ljuboje Lukic[1], David Juncker[2], and Teodor Veres[1]*

[1]National Research Council of Canada, 75 de Mortagne, Boucherville, Quebec, J4B 6Y4, Canada

[2]Biomedical Engineering Department, McGill University, 740 Dr Penfield Avenue, Montreal, Quebec, H3A 0G1, Canada

1. Analytical modeling of particle interspacing in hydrodynamically focused flows (2D approximation)

The parabolic profile of the velocity u(x) of the Newtonian liquid flowing at low Reynolds numbers in a high aspect ratio microfluidic channel is given by[1]

$$u(x) = \frac{4U_0}{a^2}x(a-x) \tag{1}$$

Where, a is the distance between the walls, x is the distance with respect to one of the walls and U_0 is the maximum velocity of the liquid in middle plane between the walls. At the bifurcation where the sheath and particle liquids are merging, after a short transitory region after the merging point, the two flows will form a steady parabolic flow where they occupy the channel in well-defined ratios Q_s/Q_{tot} for the sheath flow and Q_m/Q_{tot} for the microparticle flow. Here, Q_{tot} stands for the total flow merging after the bifurcation that is $Q_{tot} = Q_m + Q_s$. A quantity of interest in our analysis is the average velocity in the fraction of liquid corresponding to the microparticle flow. Considering this fraction is occupying the channel up to the coordinate x, we can then write that

$$u_{avg}(x) = \frac{q_m(x)}{xh} = \frac{1}{xh}\int_0^x u(y)dy \tag{2}$$

with h the height of the merging channel after the bifurcation. After solving the integral above we obtain

$$u_{avg}(x) = \frac{3Q_{tot}x}{a_2 h}\left(1 - \frac{2x}{3a}\right) \tag{3}$$

In this equation, the distance x corresponds to

$$x = \frac{Q_m a}{Q_m + Q_s} \tag{4}$$

If the interparticle spacing is ϵ_m in the incoming microparticle flow and ϵ in the merging channel after bifurcation, then the equation of continuity for the microparticle flow leads to

$$\frac{u_m \Delta t}{\epsilon_m} = \frac{u_{avg}(x)\Delta t}{\epsilon(x)} \tag{5}$$

therefore

$$\epsilon(x) = \frac{\epsilon_m a h}{Q_m}u_{avg}(x) \tag{6}$$

For $Q_s = 0$, that is no sheath flow, $x = a$ and as expected $\epsilon(a) = \epsilon_m$ since $u_{avg}(a) = Q_m/ah$. For 3D flows (low aspect ratio) we introduce an empirical factor ζ to account for the deviation from the parabolic shape of the flow near the in-plane walls of the merging channel:

$$\epsilon(x) = \zeta \frac{\epsilon_m a h}{Q_m} u_{avg}(x) \tag{7}$$

As for the distance between the stream of particles and the wall of the merging channel, we can simply approximate

$$d_w(x) = \frac{a Q_m}{2 Q_{tot}} \tag{8}$$

Both incoming streams of particles in the microparticle channel as well as the ones in the hydrodynamically focused stream are considered perfectly centered. The best fit of the experimental data in Figure 3 suggested a value $\zeta = 1.31$ for the channel geometry employed in our work.

2. Additional Table and Figures

Table S1. Comparison of passive encapsulation strategies and single-cell analytics

Encapsulation strategies	**Particle size and cells**	**Co-encapsulation**	**Key characteristics and applications**	**Reference**
Dean flow	HL60 and K562	-	High yield cell ordering and deterministic cell-in-droplet encapsulation	Kemna et al.[2]
Inertial forces	10 μm, algae cell	Beads and beads, Cells and cells	Co-encapsulation of self-ordered microparticles and a single-cell microalgae encapsulation	Lagus et al.[3]
Generic droplet microfluidics	Jurkat cells	-	Encapsulating cells in agarose droplets and cytokine detection using functionalized capture beads	Chokkalingam et al.[4]
Centrifugal fields	Jurkat cells, mouse neural stem cells	-	Cell encapsulation in hydrogel microbeads using centrifugation	Onoe et al.[5]
Dean flow	20 μm; K562, 293T, and NIH/3T3	-	High-throughput single-cell RNA-sequencing	Moon et al.[6]
Dean flow	10 μm, 30 μm; HEK293T and NIH3T3	Cells and beads	Dean flow-assisted cell and bead encapsulation for single cell expression profiling	Li et al.[7]
Droplet splitting	HT-29	-	Cell-triggered splitting to achieve for deterministic single-cell encapsulation	Zhou et al.[8]
Viscoelastic	20 μm	-	Co-encapsulation of particles using viscoelastic encapsulation	Shahrivar et al.[9]
Hydrodynamic draining	Leukemia cells K562	Cells and cells	Fluid draining technique to achieve close packing of cells	Luo et al.[10]
Dean flow and channel resistance	10 μm, 15 μm; MDA-MB-231	-	Flow resistance-based on-chip sample enrichment	Tang et al.[11]
Inertial focusing and sheath flow	15 μm; Jurkat cells	Cells and magnetic beads	Analytical modeling and 3D numerical simulation with sheath flow On-chip sample dilution for modulating λ values Co-encapsulation of THP-1 monocytes and magnetic beads for cytokine detection	Our approach

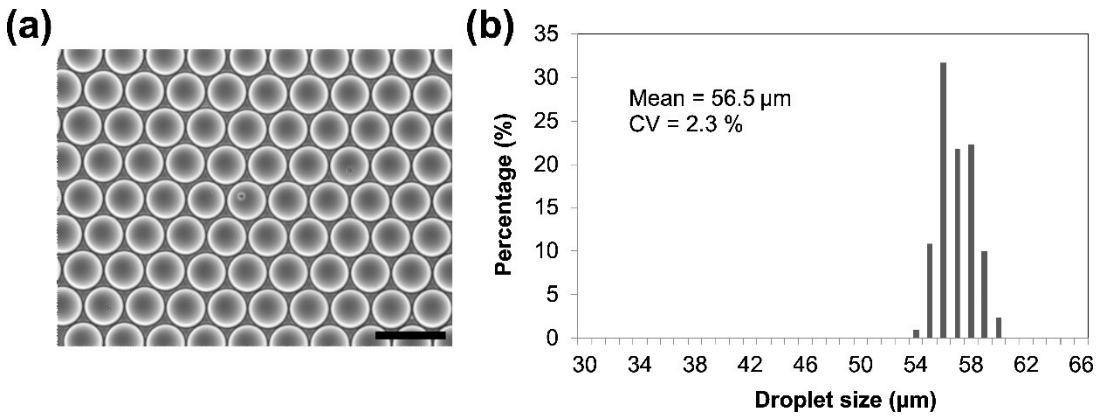

Figure S1: (a) A bright-field image of generated monolayer droplets. The scale bar is 100 µm. (b) A histogram showing droplet diameter distribution. Highly monodisperse droplets are generated using the spiral channel microfluidic device (n= 211 droplets).

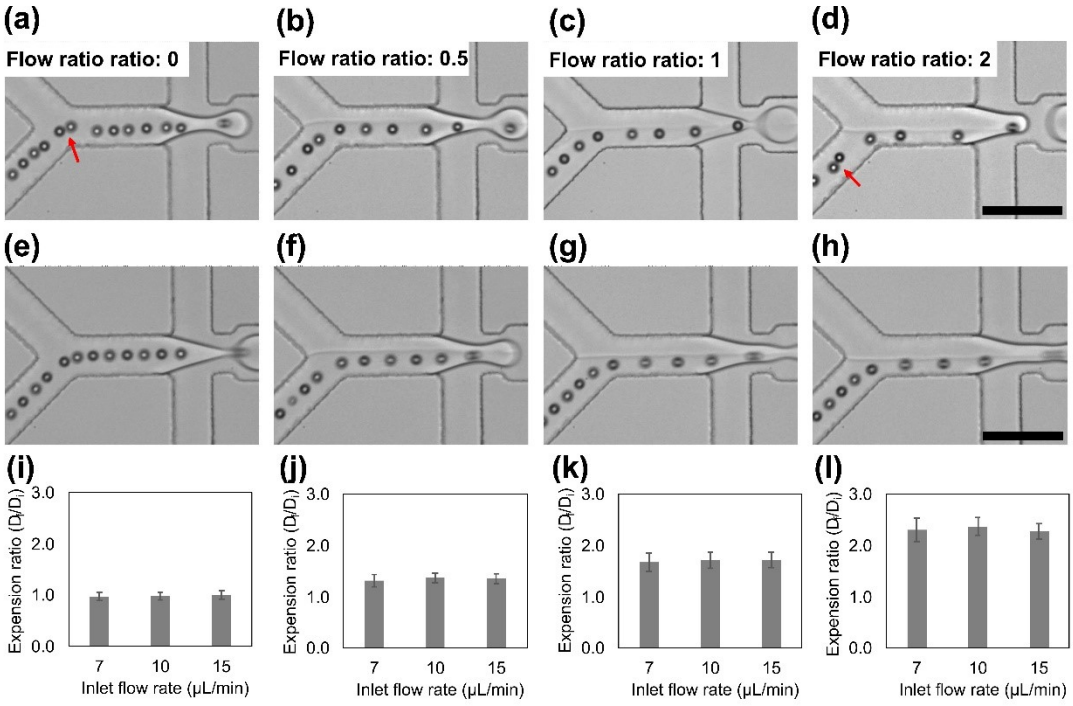

Figure S2: Hydrodynamic control of microparticle stability under different inlet flow rate conditions. Microparticles were introduced at flow rates of 7 µL/min (a-d), 10 µL/min (Fig. 3a-d), and 15 µL/min (e-f). The sheath flow was applied at 0, 3.5, 7, and 14 µL/min in (a–d), and at 0, 7.5, 15, and 30 µL/min in (e-f), respectively. Of note that at 7 µL/min, the microparticles begin to deviate from the inertially focused ordering, as indicated by the arrows. The scale bars are 100 µm. Plots of the microparticle expansion ratio at flow rate ratios of 0, 0.5, 1, and 2 are shown in (i–l), respectively (n=15). The expansion ratio of D_f/D_i, where D_i and D_f are interparticle distances before and after the Y-junction, respectively, was used to measure the change in interparticle spacing.

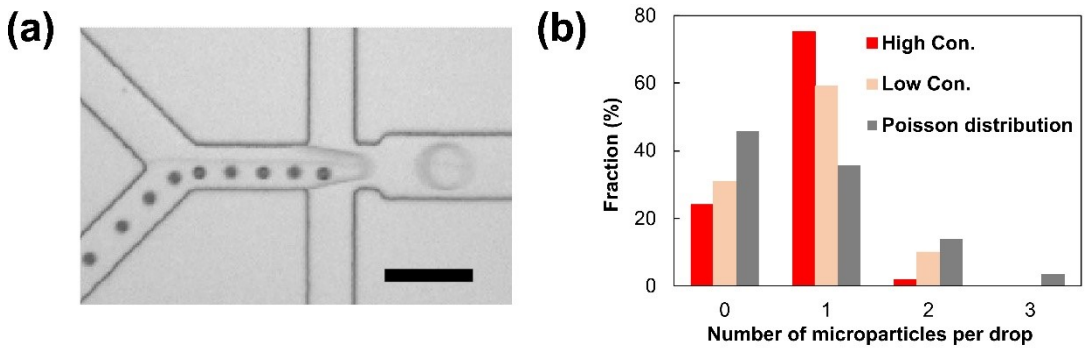

Figure S3: On-chip control of λ values under different initial conditions. (a) Microparticle distribution at a sheath flow rate of 5 µL/min. The initial microparticle concentration is approximately 14×10^6 particles/mL. The scale bar is 100 µm. (b) Comparison of encapsulation rates at two initial concentrations, 20×10^6 particles/mL (high) and 14×10^6 particles/mL (low). The high concentration condition used the sheath flow rate at 20 µL/min (see the Figures 3(d) and 4(d) in the main text). The resulting λ values are 0.78 and 0.79 at high and low initial concentrations. The Poisson distribution is plotted only for λ = 0.78.

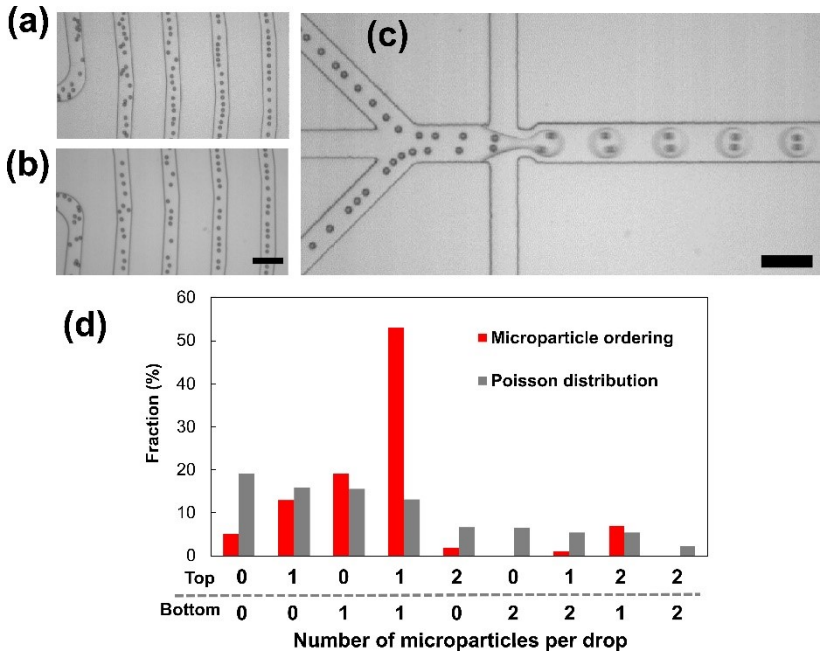

Figure S4: (a-b) Images of the microparticles self-ordering in the spiral channel loop, leading to one-to-one microparticle co-encapsulation at the junction. The aqueous phase solutions with suspended microparticles and the oil phase are introduced at flow rates of 10 µL/min and 50 µL/min, respectively. (c) Co-encapsulation of the microparticles in droplets. (d) Histogram shows double Poisson distribution and experimental co-encapsulation results, where numbers of 0, 1 and 2 represents number of particles encapsulated in the droplets (n=264 droplets, λ=0.84 and 0.82 at top and bottom channels, respectively). The scale bars are 100 µm.

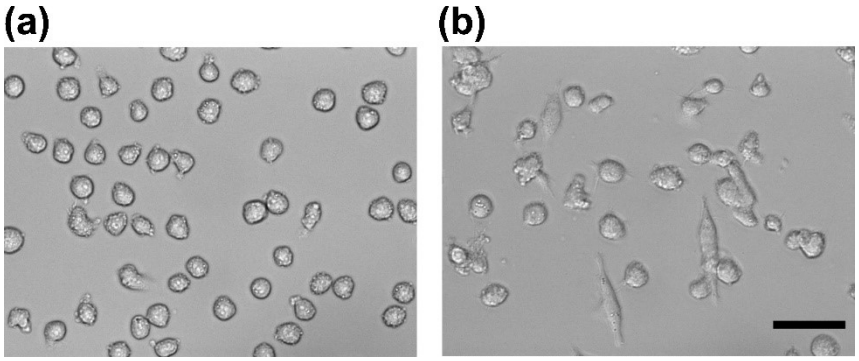

Figure S5: Morphology changes of the THP-1 cells. (a) Before (b) after the PMA/LPS stimulation. The scale bar is 100 µm.

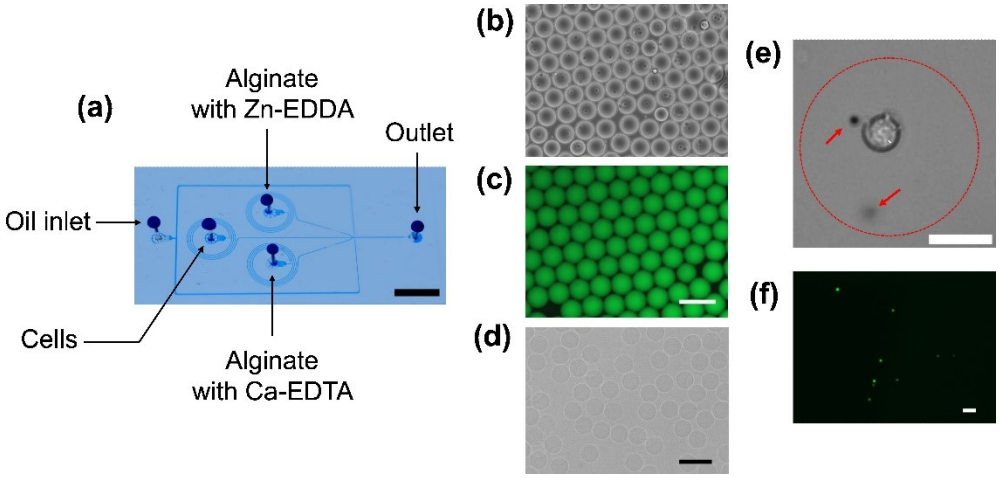

Figure S6: Alginate hydrogel formation. (a) A color dye filled microfluidic chip used for alginate droplet generation. The scale bar is 5 mm. The applied flow rates for oil, cell suspension, alginate with Zn-EDDA and alginate with Ca-EDTA solutions, are 30, 10, 0.2 and 0.2 µL/min, respectively. (b) Encapsulated cells on the alginate droplets. The resulting droplet size is approximately 54 µm ± 1.6, maintaining a low coefficient of variation (CV = 2.9%). (c) Images of FITC-dextran added alginate droplet. A distinct and homogenous distribution of alginate hydrogel is confirmed by introducing FITC-dextran into a solution. The scale bar is 100 µm. (d) Image showing collected alginate hydrogels following the oil removal process. The scale bar is 100 µm. (e) Single cell and magnetic beads co-encapsulation in an alginate droplet. The image visually presents the co-encapsulation of a THP-1 cell with two magnetics beads positioned at different planes. Dashed circle represents boundary of the droplet. Red arrow bars indicate magnetic beads. (f) Florescence images of the detected cytokine on the magnetic beads. The scale bars are 20 µm in (e-f).

3. Supporting Information Movies

Supporting Information Movie 1:

The movie shows self-ordered microparticle encapsulation without sheath flow. The flow rates of the microparticle suspension, sheath flow and oil inlets are 10 μL/min, 0 μL/min and 50 μL/min, respectively. The video is recorded at a frame rate of 24,000 fps.

Supporting Information Movie 2:

The movie shows self-ordered microparticle encapsulation with sheath flow. The flow rates of the microparticle suspension, sheath flow and oil inlets are 10 μL/min, 10 μL/min and 50 μL/min, respectively. The video is recorded at a frame rate of 24,000 fps.

4. References

1 H. 1. Bruus, *Oxford University Press*, 2008, Oxford.

2 E. W. M. Kemna, R. M. Schoeman, F. Wolbers, I. Vermes, D. A. Weitz and A. Van Den Berg, *Lab Chip*, 2012, 12, 2881–2887.

3 T. P. Lagus and J. F. Edd, *RSC Adv.*, 2013, 3, 20512–20522.

4 V. Chokkalingam, J. Tel, F. Wimmers, X. Liu, S. Semenov, J. Thiele, C. G. Figdor and W. T. S. Huck, *Lab Chip*, 2013, 13, 4740–4744.

5 H. Onoe, K. Inamori, M. Takinoue and S. Takeuchi, *RSC Adv.*, 2014, 4, 30480–30484.

6 H. S. Moon, K. Je, J. W. Min, D. Park, K. Y. Han, S. H. Shin, W. Y. Park, C. E. Yoo and S. H. Kim, *Lab Chip*, 2018, 18, 775–784.

7 L. Li, P. Wu, Z. Luo, L. Wang, W. Ding, T. Wu, J. Chen, J. He, Y. He, H. Wang, Y. Chen, G. Li, Z. Li and L. He, *ACS Sens.*, 2019, 4, 1299–1305.

8 J. Zhou, A. Wei, A. Bertsch and P. Renaud, *Lab Chip*, 2022, 22, 4841–4848.

9 K. Shahrivar and F. Del Giudice, *Soft Matter*, 2022, 18, 5928–5933.

10 X. Luo and A. P. Lee, *Microfluid. Nanofluidics*, 2023, 27, 1–12.

11 T. Tang, H. Zhao, S. Shen, L. Yang and C. T. Lim, *Microsyst. Nanoeng.*, 2024, 10, 1–12.